# Investigating the nematic–smectic-$A$ transition by capillary-length measurements near an apparent tricritical point

Nancy Tamblyn
*Department of Physics, Simon Fraser University, Burnaby, British Columbia, Canada V5A 1S6*

Patrick Oswald
*Laboratoire de Physique, Ecole Normale Supérieure de Lyon, 46, allée d'Italie, 69364 Lyon Cedex 07, France*

Angelo Miele
*Department of Physics, Simon Fraser University, Burnaby, British Columbia, Canada V5A 1S6*

John Bechhoefer
*Department of Physics, Simon Fraser University, Burnaby, British Columbia, Canada V5A 1S6*

(Received 28 October 1994)

What is the order of the nematic–smectic-$A$ ($NA$) transition? The answer to this question has flip-flopped over the years as ever more sophisticated theories and ever more careful experiments have addressed the issue. The Landau theory predicts that the transition can be either first or second order, depending on material parameters. de Gennes and McMillan [Solid State Commun. **10**, 753 (1972); Phys. Rev. A **4**, 1238 (1971)] showed that nematic fluctuations would drive the transition to first order as the temperature of the $NA$ transition approached that of the nematic-isotropic transition. Halperin, Lubensky, and Ma [Phys. Rev. Lett. **32**, 292 (1974)] (HLM) then argued that the effect of nematic fluctuations is more subtle and concluded that the transition is always at least weakly first order. Monte Carlo simulations indicate, however, that for a large enough nematic range, the transition becomes second order. We investigate the order of the $NA$ transition experimentally by measuring the capillary length (ratio of the surface tension to the latent heat) near an apparent tricritical point in a binary liquid-crystal mixture. Our measurements confirm the existence of the extra free-energy term predicted by the HLM theory and yield, as a by-product, surface-tension measurements of the $NA$ interface. Although we cannot currently detect the tricritical point suggested by numerical work, we have not approached any fundamental sensitivity limits either.

PACS number(s): 64.70.Md, 61.30.Cz

## I. INTRODUCTION

In a nematic liquid crystal, molecules have orientational but not positional ordering. In a smectic-$A$ liquid crystal, molecules are layered, forming a one-dimensional stack of two-dimensional fluids, with molecules normal to the layers. The transition between the two phases [the nematic–smectic-$A$ ($NA$) transition] would thus seem to be simple: an orientationally ordered phase becomes layered. In fact, the $NA$ transition has turned out to be one of the most subtle phase transitions yet encountered and despite nearly 25 years of intensive study, eludes complete understanding. As a recent review by de Gennes and Prost concludes, "It seems that we almost understand, but not quite" [1]. (For other reviews of the $NA$ transition, see [2–4].)

One of the subtle points concerns the order of the phase transition. At issue is whether the $NA$ transition can be second order and if so, what is the nature of the tricritical point dividing first- and second-order $NA$ transitions. The simplest Landau theories of transitions to layered states [5] suggested that the transition could be either first or second order, depending on material parameters. Early theoretical discussions by de Gennes [6] and McMillan [7] considered the increase of molecular alignment that accompanies the transition and concluded that as $T_{NA} \to T_{NI}$, there would be a tricritical point, where the transition would change from second order to first order. (Here $T_{NA}$ is the transition temperature between the nematic and smectic-$A$ phases, while $T_{NI}$ is the transition temperature between the nematic and isotropic-fluid phases. We will be discussing materials with the phase sequence $A$-$N$-$I$ encountered on increasing the temperature.) A more elaborate calculation by Halperin, Lubensky, and Ma (HLM) concluded that nematic orientational fluctuations implied that the transition would always be first order, whatever the value of $T_{NA}/T_{NI}$ [8]. Several years later, however, Monte Carlo simulations by Dasgupta and Halperin [9,10] and by Bartholomew [11] suggested that for small enough $T_{NA}/T_{NI}$, the transition should in fact be second order. This conclusion is consistent with analytical studies that show that as the splay elasticity ($K_1$) constant becomes infinite (a limit that crudely corresponds to having an infinite nematic range), the $NA$ transition should be second order and in the same universality class as the three-dimensional $XY$

 

model [3].

As for experiments, there are many examples of $NA$ transitions that are clearly first order and many examples that are apparently second order, the problem of course being that it is impossible, on account of experimental noise and uncertainties, to rule out arbitrarily weak discontinuities in thermodynamic quantities. One way to systematically investigate the theoretical models mentioned above is to measure the $NA$ latent heat as a function of the ratio $T_{NA}/T_{NI}$. Such a study was undertaken by Marynissen *et al.* for mixtures of the liquid crystals 8CB and 10CB ($n$CB is $n$-alkyl-cyanobiphenyl), where $T_{NA}/T_{NI}$ is a continuous function of the relative concentration of the two species [12]. (See Fig. 1 for a phase diagram of this mixture.) Marynissen *et al.* found an apparent tricritical point at 0.31 mole fraction of 10CB in 8CB. Near this point, the latent heat vanished quadratically with the mole fraction of 10CB, although de Gennes's theory predicts a linear dependence. More important, there is no theory that predicts a quadratic dependence. As Anisimov and his collaborators realized [13], a possible explanation is that the apparent quadratic behavior is actually a signature that the free energy contains an extra term that, while forbidden by the simplest Landau theories, appears naturally in the more sophisticated calculation by Halperin, Lubensky, and Ma. To explore this possibility, Anisimov *et al.* [14] reanalyzed the latent-heat data of Marynissen and others [12,15,16] and showed that the data were consistent with theoretical predictions for the latent heat derived from the HLM theory. More recently, Cladis *et al.* approached the same question by measuring the kinetic coefficient of $NA$ fronts in the same liquid-crystal systems [17]. (The kinetic coefficient relates the speed of a moving interface to the undercooling below $T_{NA}$; it diverges as the transition becomes weakly first order.) They also found results consistent with the HLM theory. The work of both groups was summarized in a joint review paper [18], where they concluded that there is reasonable evidence that fluctuations do keep the transition first order. There was no evidence for or against the tricritical point predicted by Monte Carlo studies.

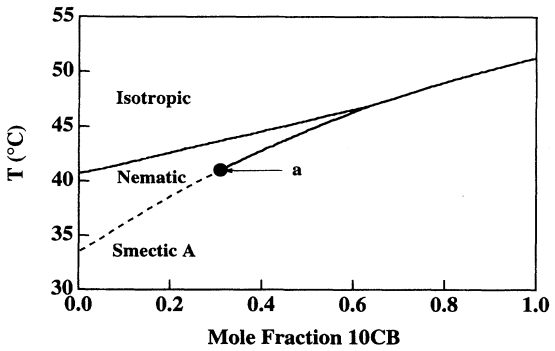


FIG. 1. Phase diagram for a mixture of 8CB and 10CB (after [12]). The transition is clearly first order to the right of the marked point, where there is a solid line, and either second order or very weakly first order to the left, where there is a dashed line.

Our purpose in this paper is to investigate the order of the $NA$ transition via a different thermodynamic quantity, the capillary length $d_0$, which is the ratio of surface tension $\gamma$ to the latent heat per unit volume $L$. The method that we use for measuring $d_0$, although familiar in the metallurgical literature [19], has been only rarely applied to liquid crystals [20]. Given a measurement of $d_0$, we can extract $\gamma$ either using experimental measurements of $L$ or by using theoretical expressions based on the HLM theory. Thus a measurement of the capillary length can be used to deduce the surface tension of the interface. By measuring the behavior of $d_0$ as a function of $T_{NA}/T_{NI}$, we can gain additional evidence concerning the order of the $NA$ transition. The sensitivity of our apparatus is currently equivalent to that of adiabatic scanning calorimeters and we do not seem to be close to any fundamental limitations of our method. Our measurements, presented below, confirm those of Anisimov and Cladis. At present, there is still no evidence for the tricritical point suggested by numerical work. We were further motivated in our study by the realization that, as far as we can determine, *no* measurements of surface tension have ever been reported for the $NA$ interface.

The rest of the paper is organized as follows. In Sec. II we review the relevant theoretical calculations. In Sec. III we describe our technique for measuring the capillary length and, using the HLM theory or using independent experimental values of the latent heat, the surface tension. In Sec. IV we describe our experimental apparatus. In Sec. V we present our measurements, while Sec. VI gives a brief conclusion. Appendix A discusses how a scratched glass substrate can produce the interface distortion we use to measure the capillary length. Appendix B discusses whether the finite thickness of the sample influences our values of the capillary length. Appendix C discusses the possible effect of using a mixture rather than a pure material for our work and of having impurities in that mixture.

## II. THEORETICAL CONSIDERATIONS

As mentioned in the Introduction, the $NA$ transition describes the spontaneous layering of molecules that were already orientationally ordered. Let the smectic layers be parallel to the $x$-$y$ plane, with molecules directed along the $z$ axis. The molecular density along the $z$ direction is

$$\rho(z) = \rho_0 \left[1 + \mathrm{Re}\left(\psi e^{iqz}\right)\right] . \quad (1)$$

Here $\rho_0$ is the average fluid density, $q$ is the smectic wave number, and $\psi$ is a complex order parameter whose magnitude indicates the strength of smectic ordering and whose phase determines the position of the layers relative to an arbitrary point along the $z$ axis. Because a uniform translation of the smectic layers should not alter the free energy, one expects that near the $NA$ transition, the free energy may be expanded in even powers of the magnitude of $\psi$. (The transformation $\psi \rightarrow -\psi$, for example, corresponds to a uniform displacement of half a

layer spacing.) For the free energy, we thus expect

$$F_A(\psi) = \frac{1}{2}A'|\psi|^2 + \frac{1}{4}C'|\psi|^4 + \frac{1}{6}E|\psi|^6. \quad (2)$$

As usual, the coefficient $A'$ is taken to be a function of temperature $A' = a(T - T_0'^*)$, while the other coefficients are taken to be independent of temperature (over the narrow range of temperatures of interest). If the coefficient $C' < 0$, the transition is first order, while if $C' > 0$, the transition is second order. The case $C' = 0$ is referred to as a Landau tricritical point.

As McMillan found for a specific model [7] and as de Gennes argued in general [21], the special properties of the nematic phase make the situation more subtle. In the nematic phase, orientational fluctuations are soft modes that cost little energy. In the smectic-$A$ phase, such fluctuations change the layer spacing and are hard modes, costing much more energy. Thus layering is necessarily accompanied by a decrease in orientational fluctuations or, equivalently, an increase in nematic order parameter. This leads to additional terms in the free energy of the form

$$F_N(S) - D\psi^2(\delta S) + \frac{1}{2\chi}(\delta S)^2, \quad (3)$$

where $F_N(S)$ is the free energy of the base nematic state, $S$ is the nematic order parameter in the absence of smectic layering, and $\delta S$ is the increase in nematic order parameter caused by the layering. The second term shows that layering becomes easier as orientational fluctuations are decreased. The third term represents the free-energy cost of having a nematic order parameter $(S+\delta S)$ higher than the equilibrium value in the absence of layering $(S)$. Minimizing the augmented free energy with respect to $\delta S$, one finds that the free energy again has the form shown in Eq. (2), with a shifted quartic coefficient $C = C' - 2D^2\chi$. The "nematic susceptibility" $\chi$ measures the free-energy cost of increasing the order parameter. Since the nematic order parameter increases as the temperature decreases below $T_{NI}$, we expect $\chi$ to be large when $T_{NA} \lesssim T_{NI}$ (since the nematic order parameter will be small before the layering, which will increase its value to close to 1). Conversely, when $T_{NA} \ll T_{NI}$, $\chi$ will be small. Thus the smaller the existence range of the nematic phase, the bigger the renormalization of the coefficient $C'$, implying that as $T_{NA} \to T_{NI}$, the transition will change from second to first order.

Halperin, Lubensky, and Ma showed that the transition from the normal to the superconducting state predicted by the BCS theory for type-I superconductors must be weakly first order by considering the partial expulsion of "blackbody radiation" from the superconducting phase [8]. Because the $NA$ transition is described by a Hamiltonian that may be mapped onto a modified version of the superconducting transition [22], it should also be a first-order transition. By including the coupling between director fluctuations $\delta\mathbf{n}(\mathbf{r})$ and the smectic order parameter $\psi(\mathbf{r})$, they showed that a transition thought to be second order below the Landau tricritical point would in fact be weakly first order. With the extra coupling terms the free-energy density becomes

$$\begin{aligned} F(\psi, \delta\mathbf{n}(\mathbf{r})) = {} & \frac{1}{2}A'|\psi|^2 + \frac{1}{4}C|\psi|^4 + \frac{1}{6}E|\psi|^6 \\ & + \frac{1}{2}c\xi_{\|}^2 \left|\nabla_{\|}\psi\right|^2 + \frac{1}{2}c\xi_{\perp}^2 \left|(\nabla_{\perp} - iq\delta\mathbf{n})\psi\right|^2 \\ & + \frac{1}{2}K\left[(\nabla\cdot\delta\mathbf{n})^2 + (\nabla\times\delta\mathbf{n})^2\right]. \end{aligned} \quad (4)$$

The first three terms of Eq. (4) are the de Gennes–McMillan free energy, with the coefficient $C$ renormalized by the $S$ coupling. The last two terms represent the elastic restoring force due to a small orientational fluctuation $\delta\mathbf{n}$. Here, for convenience of calculation, we are assuming that the Frank elastic coefficients for splay, twist, and bend are all equal to $K$. (This simplification does not alter any of our conclusions.) The $\nabla_{\|}$ term accounts for changes in the layer spacing and the $\nabla_{\perp} - iq\delta\mathbf{n}$ term accounts for rotations of the molecules with respect to the layers, which may themselves be rotated with respect to the $x$-$y$ plane. The constants $\xi_{\|}$ and $\xi_{\perp}$ are the parallel and perpendicular correlation lengths and $c$ is a phenomenological constant with units of energy per unit volume. In Eq. (4), smectic-layer fluctuations $\psi$ are coupled to nematic fluctuations $\delta\mathbf{n}$. The basic assumption of HLM is that the smectic fluctuations are smaller than the nematic ones. Physically, this makes sense near the Landau tricritical point. Since the nematic order parameter $S$ is small, there will be large fluctuations of $\delta\mathbf{n}$ about the $z$ axis. Mathematically, the approximation consists of letting $\psi$ be constant (so that all $\nabla\psi$ terms are zero) and then integrating out the $\delta\mathbf{n}$ field in the free energy. If $\psi$ is constant, the free-energy density is

$$\begin{aligned} F(\psi, \delta\mathbf{n}) = {} & \frac{1}{2}A'|\psi|^2 + \frac{1}{4}C|\psi|^4 + \frac{1}{6}E|\psi|^6 \\ & + \frac{1}{2}c\xi_{\perp}^2 q^2 (\delta n)^2 |\psi|^2 \\ & + \frac{1}{2}K\left[(\nabla\cdot\delta\mathbf{n})^2 + (\nabla\times\delta\mathbf{n})^2\right]. \end{aligned} \quad (5)$$

One can evaluate $[\delta n(r)]^2$ by Fourier transforming it into $k$ space, where $[\delta n(r)]^2 \sim \int d\mathbf{k}[\delta n(k)]^2$. The free-energy terms involving $[\delta n(r)]^2$ are then

$$F\{\psi, [\delta n(k)]^2\} \sim \int d\mathbf{k}\left[\frac{1}{2}c\xi_{\perp}^2 q^2|\psi|^2 + \frac{1}{2}Kk^2\right][\delta n(k)]^2. \quad (6)$$

Using the equipartition theorem for each mode $[\delta n(k)]^2$, we have

$$[\delta n(k)]^2 \sim \frac{k_B T}{Kk^2 + c\xi_{\perp}^2 q^2|\psi|^2}. \quad (7)$$

This expression is then Fourier transformed back into real space, giving

$$[\delta n(r)]^2 \sim \int_0^{k_{max}} dk \frac{k^2(k_BT)}{Kk^2 + c\xi_\perp^2 q^2|\psi|^2} = \int_0^{k_{max}} dk \frac{k_BT}{K} - \int_0^{\infty} dk \frac{k_BTc\xi_\perp^2 q^2|\psi|^2}{K(Kk^2 + c\xi_\perp^2 q^2|\psi|^2)} . \quad (8)$$

Here the divergent part of the Fourier-transform integral has been cut off at $k_{max}$ and the finite part has been extended to $k = \infty$. Substituting this expression for $[\delta n(r)]^2$ back into the free energy [Eq. (5)], we find that first term renormalizes the coefficient $A'$ and thus shifts the transition temperature. The effect of the second term is more dramatic, since the free energy now has a term that is cubic in $|\psi|$. The effective free energy is

$$F(\psi) = \frac{1}{2}A|\psi|^2 + \frac{1}{3}B|\psi|^3 + \frac{1}{4}C|\psi|^4 + \frac{1}{6}E|\psi|^6, \quad (9)$$

where

$$B = -\frac{3\pi}{2}\frac{k_BT_{NA}c^{3/2}\xi_\perp^3 q^3}{K^{3/2}}. \quad (10)$$

Because $B$ is always less than zero, we conclude that the transition is first order. Because $B$ is small, one can foresee very weak first-order transitions.

The new cubic term in the free energy apparently violates the symmetry with respect to uniform translations that was invoked when expanding the free energy in even powers of $|\psi|$. In fact, translation symmetry merely requires that the free energy not involve explicitly the phase of the complex order parameter $\psi$. We exclude terms $\sim |\psi|^\alpha$, with $\alpha \neq \{0, 2, 4, ...\}$ on the grounds that we expect the free energy to be analytic near $\psi = 0$. The $|\psi|^3$ term is thus usually forbidden because it is not analytic. We begin with a free energy that is a function of both $\psi$ and $\delta\mathbf{n}$ and which meets the requirements of both symmetry and analyticity. By integrating out the nematic fluctuations, we are projecting the two-order-parameter free energy $F(\psi, \delta\mathbf{n})$ onto the single-order-parameter, effective free energy $F(\psi)$. Because this free energy is merely an approximation to the full one, it need not be analytic in $\psi$.

Another important consequence of integrating out the nematic fluctuations and taking them to be Gaussian is that we have assumed that they are large compared to smectic fluctuations. This is a good approximation for type-I smectics (the analog of type-I superconductors), but it is questionable for type-II smectics. In the extreme type-II limit ($K$ large), orientation fluctuations are suppressed ($\delta\mathbf{n} \to \mathbf{0}$) and the free energy should revert back to the form of Eq. (2). In this case, if $C > 0$, one would have a second-order transition. As the smectic becomes more strongly type II, one cannot decouple the $\delta\mathbf{n}$ field from the $\psi$ field. The resulting partition function has been evaluated numerically via Monte Carlo simulations by Dasgupta and Halperin and by Bartholomew, who concluded that for strongly enough type-II smectics, the transition should be second order. Little is known about the type of tricritical point that would divide the regime of first-order transitions from the regime of second-order transitions.

## III. CAPILLARY-LENGTH MEASUREMENTS

The simple Landau theory for the $NA$ transition (and also the modification of it by de Gennes) predicts that the surface tension $\gamma$ goes very quickly to zero as one approaches the Landau tricritical point. Because the surface tension goes to zero more quickly than the latent heat, the capillary length $d_0 = \frac{\gamma}{L}$ should also go to zero at the tricritical point. If the HLM theory does hold, then none of these quantities should actually vanish.

The problem becomes one of trying to measure either the surface tension or the capillary length in one of these mixtures. Traditional methods of measuring surface tension do not work very well here. They require a large quantity of the materials and large surface tensions. The surface tensions in this experiment are expected to become very small near the Landau tricritical point. The slow decrease of the capillary length makes it a better candidate for measurement.

Fortunately, there is a technique from metallurgy, introduced by Schaefer *et al.*, that allows direct measurement of the capillary length [19]. When a metal is solidifying, domains of different crystal lattice orientation grow together, meeting at grain boundaries. The surface tension of the solid-liquid interface is different from the surface tension of the solid-solid surface at the grain boundary. Since the forces must balance at the point where liquid, solid, and grain boundary meet, the solid-liquid interface will make contact with the grain boundary at an angle. [See Fig. 2(a).] The effect is entirely analogous to the creation of a meniscus of coffee in a cup, where the flat interface imposed by the gravitational field bends the fluid upward to make contact with the sidewalls. In the present case, the flat interface away from the grain boundaries is imposed by a thermal gradient.

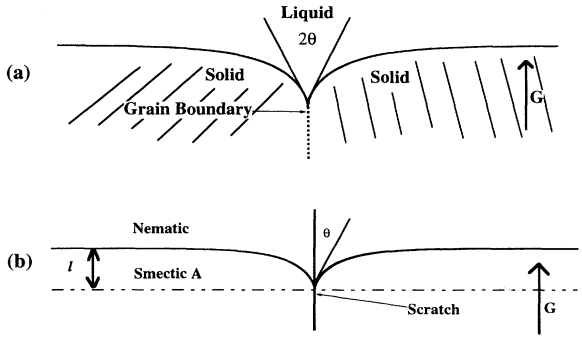


FIG. 2. (a) A solid-liquid interface in a temperature gradient. The energy of the grain boundary in the solid phase pulls on the interface, creating a cusp whose size $\ell \approx (d_0T_0/G)^{1/2}$. (b) A smectic-A–nematic interface in a temperature gradient. The local melting of the smectic phase over the scratch produces a cusp in the interface that is identical in form to that produced by the solid grain boundary in (a).

At first thought, one would conclude that the method of Schaefer *et al.* for measuring the capillary length would not work for the $NA$ interface because there is no analog of the notion of grain boundary in the laterally isotropic Sm-$A$ phase. But we found that a cusp could nonetheless be created by a scratch on the substrate surface. [See Fig. 2(b).]

One might justifiably wonder just how a scratch on one of the glass plates produces a cusp. Our view of the situation was inspired by observations and discussion of the effect of rough surfaces on nematic alignment. (See the references cited in [23].) In that case, the nematic order parameter decreases sharply in the vicinity of a rough glass surface. Barbero and Durand [23] showed that for small surface distortions, the sample remains nematic throughout and has elastic distortion energy. For large surface distortions, the nematic melts near the surface, eliminating the elastic energy at the cost of the extra free energy required to create the isotropic phase at temperatures at which the nematic phase is stable. The crossover occurs for distortions on the scale of the nematic correlation length $\xi \approx 100$ Å. Moreover, the roughness-induced melting penetrates into the nematic over this same length scale $\xi$.

For a smectic, the tradeoffs are similar. At a given temperature, the system can remain smectic at the cost of smectic-elastic deformation energy. Alternatively, it can revert to a nematic, paying the free-energy cost of having a metastable phase. The result is that locally the $NA$ transition temperature is depressed. Because of the horizontal temperature gradient used in our experiments, the interface will sit at a different position over the scratch, as compared to the interface away from the scratch, leading to the cusps we see. One difference with the nematic case is that the relevant length scale is much larger (about 15 $\mu$m) than it is for nematics, reflecting the well-known sensitivity of smectics to elastic distortion [1]. In Appendix A, we estimate the magnitude of this effect and find reasonable agreement with measured cusp depths.

The experiment then consists of placing a liquid crystal between two glass plates in a temperature gradient, thereby creating the reference flat interface. Since one of the plates is scratched, the interface will form a cusp centered on the scratch. From the shape of the cusp, which we now derive, we can deduce the capillary length.

### A. Measurement of the capillary length from cusp images

The key point of physics lies in the Gibbs-Thomson law, which states that the coexistence temperature of a curved interface deviates slightly from its equilibrium value [24,25]. In particular, $T(\kappa) = T_{NA}\,(1 - d_0\kappa)$, where $\kappa$ is the local mean curvature of the interface. The physical interpretation of this effect is that the surface tension of the interface squeezes on the interior phase, raising its pressure and (via the Clausius-Clapeyron law) shifting its equilibrium coexistence temperature. If the local interface position relative to that of a flat, undisturbed interface is given by $y$, then the drop in transition temperature at each point on the interface is $Gy$. Since the curvature is expressed in terms of $y$ by $\kappa = y''/(1+y'^2)^{3/2}$, the assumption that each point of the interface is in local thermodynamic equilibrium leads to the nonlinear differential equation

$$Gy = \frac{T_{NA} d_0 y''}{(1+y'^2)^{3/2}}. \tag{11}$$

By scaling both $x$ and $y$ by $\ell = \sqrt{\frac{T_{NA} d_0}{G}}$, we can remove all material parameters from Eq. (11), leading to the equation

$$y = \frac{y''}{(1+y'^2)^{3/2}}, \tag{12}$$

where $x$ and $y$ are now understood to be scaled variables. The length $\ell$ sets the basic scale of the cusp. In our experiments, it was typically 5 – 50 $\mu$m, depending on the mixture concentration and on the temperature gradient. Equation (12) may be integrated by multiplying both sides by $y'$ to get

$$y' = \sqrt{\frac{1}{(\frac{y^2}{2} + f)^2} - 1}\,. \tag{13}$$

Since $y' = 0$ when $y = 0$ (far away from the scratch), we must fix the integration constant to be $f = \pm 1$. In order that $y'$ be real, we choose $f = -1$. Integrating from the bottom of the cusp $y_0$ to $y$ and from 0 to $x$, we find

$$x = x_0 + \ln\left(\frac{1 + \sqrt{1 - \frac{(y-y_0)^2}{4}}\sqrt{1-\sin\theta}}{\frac{y-y_0}{2}\left(\sqrt{1+\sin\theta} + \sqrt{2}\right)}\right) - 2\left(\sqrt{1 - \frac{(y-y_0)^2}{4}} - \sqrt{\frac{1+\sin\theta}{2}}\right). \tag{14}$$

Using the other boundary condition $y'(y = y_0) = \frac{1}{\tan\theta}$, we find $y_0 = \sqrt{2(1-\sin\theta)}$. This describes the interface shape in terms of the contact angle $\theta$. Fitting the functional form of the cusp to the interface coordinates for a number of different images resulted in about a 10% spread in the parameter values for the capillary length.

### B. Calculation of the latent heat, surface tension, and capillary length from the HLM theory

The measured values of $d_0$ were fit to a theoretical function calculated according to the HLM theory. We found it more convenient to calculate the surface tension and the latent heat separately and then to take their ratio. The latent heat is [18]

$$\left(\frac{\Delta S}{\Delta S^*}\right) - \left(\frac{\Delta S}{\Delta S^*}\right)^{-\frac{1}{2}} = \frac{3}{8}\left(\frac{a}{\Delta S^*}\right)\left(\frac{C_0}{E}\right)(X - X^*), \tag{15}$$

where $X$ is the concentration of 10CB and $C = -C_0(X -$

$X^*$), an expression that is valid near the Landau tricritical point. The jump in entropy is $\Delta S = L/T_{NA} = (\partial F/\partial T)_{T_{NA}} = a\psi^2/2$. Quantities denoted by an asterisk ($\Delta S^*$, $X^*$) refer to values taken on at the Landau tricritical point. We define $\Delta S/\Delta S^* \equiv \Delta S' = (\psi/\psi^*)^2$. From Eq. (15), we extracted the reduced entropy jump $\Delta S'$ as a function of the concentration $X$ by Newton's method [26].

The surface tension is given by

$$\gamma = c\xi_\perp^2 \int_{-\infty}^{\infty} \left(\frac{d\psi}{dx}\right)^2 dx \qquad (16)$$
$$= \xi_\perp \sqrt{2c} \int_0^{\psi} \sqrt{F(\psi)}\, d\psi,$$

with $F(\psi) = (A/2)|\psi|^2 + (B/3)|\psi|^3 + (C/4)|\psi|^4 + (E/6)|\psi|^6$. Using Eq. (15) and writing the coefficients $A$, $B$, and $E$ in terms of $C$ and $\psi^*$, we can rewrite the surface tension as

$$\gamma = 4\xi_\perp \left(\frac{cE}{3}\right)^{1/2} \left(\frac{\Delta S^*}{a}\right)^2 \times \int_0^{\sqrt{\Delta S'}} d\psi' \left[\left(2\sqrt{\Delta S'} + \Delta S'^2\right)\psi'^2 - 4\psi'^3 - 2\left(\Delta S' - \frac{1}{\sqrt{\Delta S'}}\right)\psi'^4 + \psi'^6\right]^{1/2}. \qquad (17)$$

Equations (15) and (17) were then used to compute $d_0$.

## IV. EXPERIMENTS

### A. Sample preparation

Our candidate system was the mixture studied by Marynissen *et al.*, 8CB and 10CB. These molecules are homologous liquid crystals, each made of a hydrocarbon chain attached to two phenyl groups and a polar cyano group. The phase diagram of the mixtures, Fig. 1, has an apparent $NA$ tricritical point. (Note that this is distinguished both from the $N$-$A$-$I$ triple point, which is present in the phase diagram and from the Landau tricritical point, which is the point along the $NA$ transition where the fourth-order Landau coefficient $C$ vanishes.)

Mixtures of 8CB and 10CB were "sandwiched" between 1-mm-thick glass plates separated by wire spacers that were typically 12.5 $\mu$m in diameter. The bottom plate measured 25 × 25 mm$^2$ and the top plate measured 20 × 20 mm$^2$. Because we prepared the mixtures using small quantities of liquid crystal (0.1 g typically), we determined the actual mixture concentrations by measuring the nematic existence range and comparing it to the phase diagram [27]. In the regime of interest, the nematic existence range varied linearly with concentration. By this method, our concentration values were accurate to 2%.

To create the cusp, we lightly scratched the bottom plate along the center using a straight edge and a tungsten-carbide scribe. The plates were thoroughly cleaned with soap in a heated, sonicated bath; rinsed with tap water, distilled water, and distilled, deionized water; and then dried in an oven at 120 °C for 1 h. In order to enforce homeotropic boundary conditions (i.e., to make the liquid-crystal molecules perpendicular to the glass plates, we coated the glass with a silane compound (Merck ZLI 2510) by dipping the plates in <0.1% silane in an equal mixture of toluene and dichloromethane. The plates were separated by spacer wires and glued at the edges. The completed cell was filled by heating it, placing a drop of 8CB-10CB mixture at the edge, and letting capillary action draw the mixture between the glass plates.

Treating the surfaces for the anchoring of the liquid-crystal molecules turned out to be the most difficult part of the sample preparation. Ideally, the surface of the glass would be perfectly flat, with a uniform monolayer of silane covalently bonded to it. Any dirt on the glass not only prevented the silane from bonding properly, but also contaminated the sample material. Heterogeneities in the sample or on the surface would pin the interface away from the proper shape. The quality of the samples also depended critically on the type of glass used to make the sample cell. In general, green-tinted, or soda-lime, glass gave the best results. Two kinds of "white" or clear glass produced interfaces far removed from the ideal perfectly straight line. A closer inspection of the glass using an atomic-force microscope (AFM) showed that the soda-lime glass was flat to within 20 Å with only long-wavelength variations, while the white glass had abrupt defects that were more pronounced. These small inhomogeneities of the surface pinned the interface in the small temperature gradients required for the experiment.

The other sensitive aspect of these samples was the scratch on the glass. Applying too much pressure on the scribe produced an uneven scratch with large distortions of the surrounding glass. Pressure that was too light did not create the abrupt corner at the edge of the scratch required to pin the interface. A closer look at a good scratch with an AFM revealed that a scratch depth of about 0.3 $\mu$m and a width of 10−18 $\mu$m usually produced the desired pinning. (See Fig. 3.)

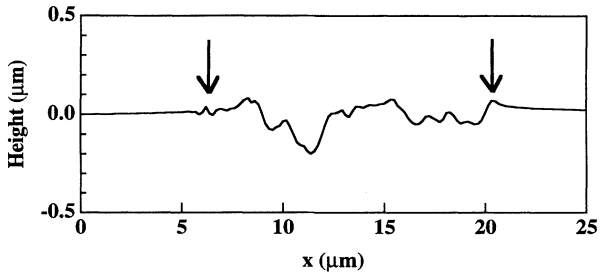


FIG. 3. Atomic-force microscope profile of a typical scratch. The interface was clearly pinned at the right-hand side. The left-hand side did not pin the $NA$ interface correctly, because an abrupt drop is needed. The shallow descent of the left-hand side of the scratch was also apparent in an optical microscope, where the interface was seen to be weakly pinned in two or three places. The vertical arrows point to the "edges" of the scratch.

### B. Apparatus

The temperature gradient for the cusp measurements was produced using two copper blocks separated by a 4-mm gap. Each block had channels cut running through it that carried water from a separate water bath [28]. One water bath was set to a temperature above the phase-transition temperature and the other to a temperature below the transition. The temperature of each block was stable to within $\pm 2$ mK over 15 min and $\pm 7$ mK over 2 h. Holding the two copper blocks at different temperatures created a linear temperature gradient across the gap, so that that the $NA$ transition would occur at a temperature reached somewhere in the middle of the gap. The sample cell described above was placed on the copper blocks, straddling the gap. It was important that the base blocks be as level as possible and that they be at the same height, so that the sample made good thermal contact with both sides. In our case, the block heights were adjusted to be within 25 $\mu$m of each other. To avoid vertical temperature gradients, we attached larger copper blocks over the sample, surrounding it, but not resting on it. This reduced the vertical gradient to less than 10% of the horizontal gradient. The blocks were cut so that there was about 50-$\mu$m clearance above the sample, to leave room for different sample thicknesses. It was important that the upper blocks not touch the sample because applying pressure on the smectic layers would compress them and form unwanted defects. The copper ovens were surrounded on the sides with a layer of Teflon and a layer of aluminum and on the top and bottom with fiberglass sheets with glass windows. The top window was double glazed, but the bottom one was not, because of the short working distance of the microscope objective. The entire apparatus was attached to an $XY$ stage that was fixed to an inverted microscope [29]. (See Fig. 4.)

The interfaces were observed by phase-contrast microscopy. A charge coupled device (CCD) camera [30] was attached to the microscope and pictures of the interface were recorded by a frame-grabber card with real-time background subtraction [31] controlled by "NIH Image" [32].

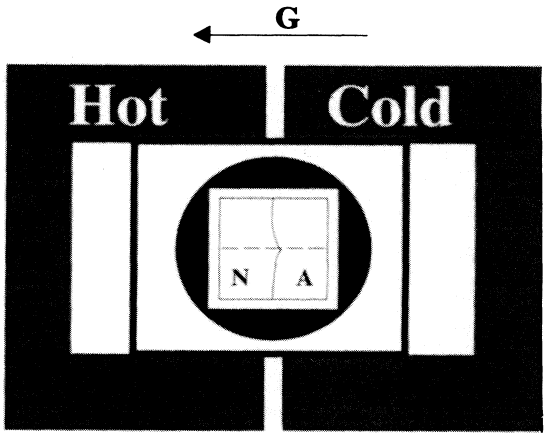


FIG. 4. Schematic top view of the temperature-gradient stage. The sample is surrounded by a disk, so that it may be rotated to align the scratch with the temperature gradient.

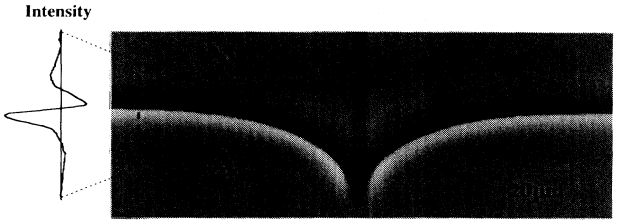


FIG. 5. Measured interface coordinates superimposed on photograph of cusp. $X = 0.585$, $h = 12.5$ $\mu$m, phase-contrast microscopy. The vertical graph shows the light-intensity profile perpendicular to the interface.

The interface position was defined to be the intersection between the intensity fringes produced by the phase-contrast optics with the average value of the background intensity, interpolated through the interface region [36], as shown in the inset to Fig. 5, which also shows a picture of a cusp with the measured interface superimposed on it.

### C. Calibration of the temperature gradient

To measure the block temperatures, we placed temperature probes (platinum resistance temperature devices, or RTDs) in the lower section of each block. To calibrate the temperature gradient in terms of these block temperatures, we allowed the apparatus to come to thermal steady state, with the interface located near the middle of the gap. The temperature of each water bath was raised by an amount roughly one-twentieth of the total temperature difference between the baths. The temperature at each RTD was read before and after this change, so that the temperature increase of the blocks could be known. This temperature rise moved the interface a distance equal to the change in temperature in the sample divided by the gradient. By knowing that the entire system had had its temperature increased uniformly by a certain amount, one could assume that the increase in the sample was the same, thus avoiding introducing into the calculation any heat losses between the RTDs and the interior of the sample. Since the temperature increase was small and the ovens well insulated, we could assume that the losses to the environment were the same before and after the temperature change. It was important that the temperature increase be small enough to keep the interface close to the center of the sample, because the gradient varied near the edges of the gap. By comparing the gradient calculated in this manner with the nominal gradient $G_{nom}$, which could be inferred by dividing the temperature difference between the RTDs by the width of the gap, we arrived at a single factor ($\alpha = 0.70 \pm 0.03$) that accounted for the losses between the RTDs and the sample interior. The gradient at the middle of the sample was then $G = \alpha G_{nom}$.

To assess the linearity of the temperature gradient over the gap between the ovens, we placed a thermocouple be-

tween two glass plates to simulate a sample. The glass plates were then slowly and smoothly pushed from one side of the gap to the other by a stepper motor [33] connected to a lead screw. The sample displacement relative to the fixed gap was measured using a linear variable differential transformer [34]. The temperature profile obtained from this endeavor was linear to 4% over most ($\approx$ the center 3 mm) of the gap. The gradient decreased by 10% in the 0.5 mm nearest each edge. When measuring $d_0$, we adjusted our bath temperatures to center the interface in the gap.

## V. RESULTS

Pictures of the cusp for a given concentration of 10CB in 8CB were taken at different temperature gradients. The mixtures were of concentrations between 0.332 and 0.585 mole fraction 10CB. An attempt was made to include a mixture of concentration 0.20, but the faintness of the interface and the interference of the phase-contrast halo around the scratch prevented the cusp, which would be small, from being clearly observed. Since our measurement is made from CCD images of the sample, the method breaks down when the interface cannot be clearly viewed.

For those mixtures which could be observed, the size of the cusp increased as the temperature gradient decreased (see Fig. 6), as one would expect from the derivation of the cusp shape, which gives $\ell \sim G^{-\frac{1}{2}}$. (See Fig. 7.) The contact angle varied between about 20° and 40° and seemed to depend not on either temperature gradient or mixture concentration, but more likely on the particular

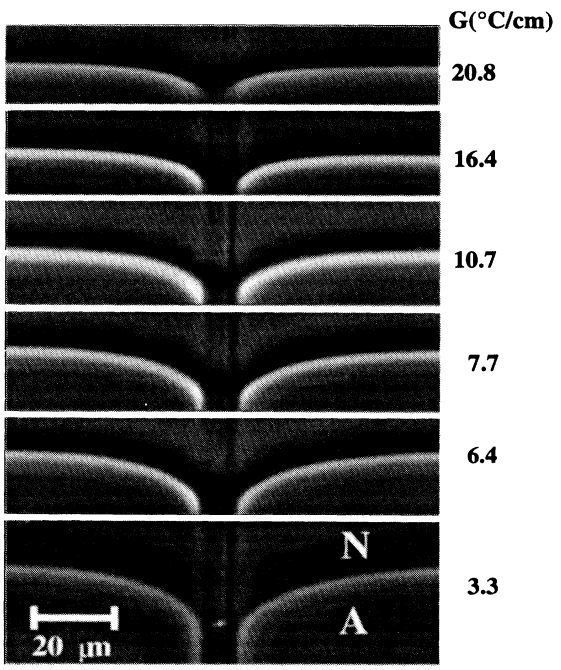


FIG. 6. Cusps in different temperature gradients. $X = 0.503$, $h = 12.5$ $\mu$m, phase-contrast microscopy.

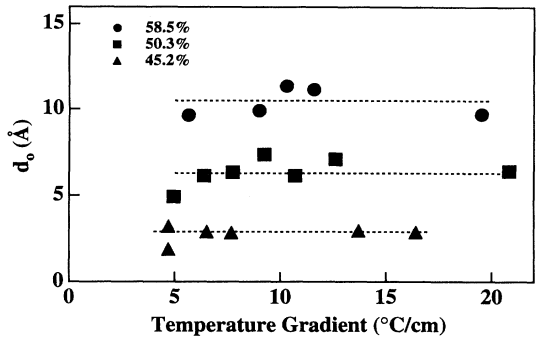


FIG. 7. Capillary lengths for three different concentrations of 10CB determined for several temperature gradients.

point at which it made contact with the scratch on the sample. (See Fig. 8.)

By fitting to a number of cusps at different gradients for each concentration, we measured values of the capillary length $d_0$ for eight different mixtures. The fitting was done using a commercial software package that uses the Levenberg-Marquardt algorithm [35]. Each cusp was fit to the function $x(y)$ derived above [Eq. (14)]. The free fit parameters were the capillary length $d_0$, the contact angle $\theta$, the height of the cusp $y_0$ (actually the asymptotic $y$ value of the interface far from the cusp), and the $x$ location $x_0$ of the point of contact to the scratch.) See Fig. 9 for a sample fit and Fig. 10 for capillary values obtained from the fit. The solid line in Fig. 10 is calculated using the parameters from this fit. These results were compared with the same function calculated using the parameters obtained by Anisimov *et al.* from the latent heat data of Marynissen *et al.* (See Table I.) The fit of the capillary-length data supports the HLM theory. It does not go linearly to zero, as one would expect from de Gennes's version of the Landau theory, and the data conform to the shape of the HLM theoretical curve.

Using the HLM expression for the latent heat [Eq. (15)], we can extract the surface tension from our capillary-length measurements. If, in this expression, we use the parameters that we deduce from our $d_0$ measurements, then the value that we obtain is a theoretical one,

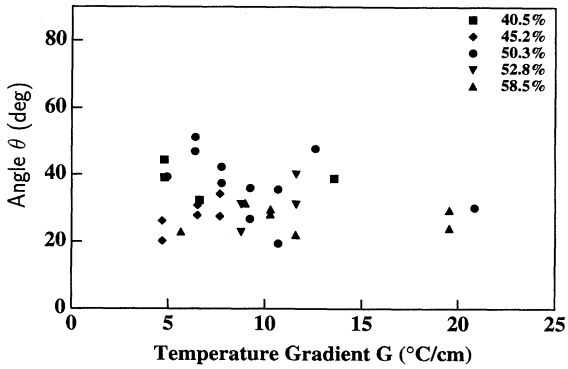


FIG. 8. Measurements of contact angle for several mixtures over a range of temperature gradients.

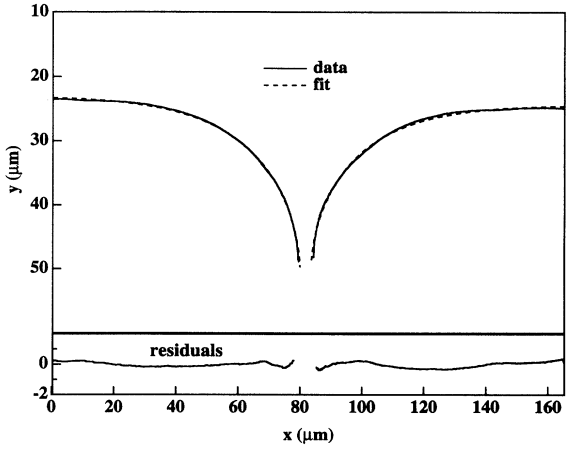


FIG. 9. Sample fit, using Eq. (17) to an interface profile. A plot of the fit residuals is at bottom. The maximum deviation is about 0.3 $\mu$m, which is to be compared to the total cusp size of 25 $\mu$m. Here $X = 0.585$, $h = 12.5$ $\mu$m, and $G = 10.3$ °C/cm. From the fit, we deduced $d_0 = 11.8$ Å and $\theta = 28.2°$.

as it assumes the validity of the HLM theory for both surface tension and latent heat for the particular material. If, as was the case, we use the parameters that Anisimov *et al.* deduced, then we do not make any such assumption, as the HLM theory in that case was shown to fit the measured latent heats well. In practice, both sets of parameter values gave similar results for the surface tension, but using the Anisimov parameters significantly reduced the uncertainty in $\gamma$ because the fit now takes into account both the $L$ and the $d_0$ data. The resulting values of $\gamma$ span four orders of magnitude. See Fig. 11 and Table II, which summarizes our data.

Throughout our discussion so far, we have neglected the vertical curvature of the meniscus found in the gap between the two plates. Because only one plate is scratched, the interface curvature might vary in the vertical direction, biasing our measurement of $d_0$. In Appendix B, we discuss this matter in detail. The upshot is that the values of $d_0$ that we measure are unaffected by the sample thickness $h$, for $h < 15$ $\mu$m. Consequently, our measurements were performed on samples with $h = 12.5$ $\mu$m.

Finally, we note that we have also assumed that our sample is a pure, single-component system, both in the discussion of the form of the free energy and of the shape of the cusp. However, we in fact use a two-component system that contains a small amount of impurities. In Appendix C, we argue that we are nonetheless justified in neglecting these and that our presentation given above is valid.

TABLE I. Parameters from fits to the HLM model of the $NA$ transition. We have written the fit parameters in terms of those used by Anisimov. Here $\Delta S^*$ is the entropy jump per mole (in the text, it is per unit volume). $R$ is the ideal gas constant. $\alpha$ is defined as $(3/8)(aC_0/E)$ and $\beta$ as $4\xi_\perp(cE/3)^{1/2}/a^2$. In our work, all four parameters were deduced by fitting $d_0(X)$. In the case of Anisimov *et al.* [18], $\Delta S^*/R$, $\alpha$, and $X^*$ were deduced from latent-heat measurements $L(X)$. The last parameter under the Anisimov column, $\beta$, was deduced from our $d_0$ data using Anisimov's data for the other parameters. Note the smaller error in $\beta$ that comes from using experimental data for the latent heat rather than deriving all quantities from the $d_0$ data alone.

| Parameter | This work | Anisimov |
|---|---|---|
| $\frac{\Delta S^*}{R}$ | 0.020±0.005 | 0.0261 |
| $\alpha$ | 1.24±0.20 | 0.993 |
| $X^*$ | 0.416±0.003 | 0.4243 |
| $\beta$ | 1800± 800 | 2180 ± 50 |

## VI. CONCLUSIONS

We have described the experimental setup and sample preparation for direct measurement of the capillary length $d_0$ of a binary liquid-crystal mixture. For different

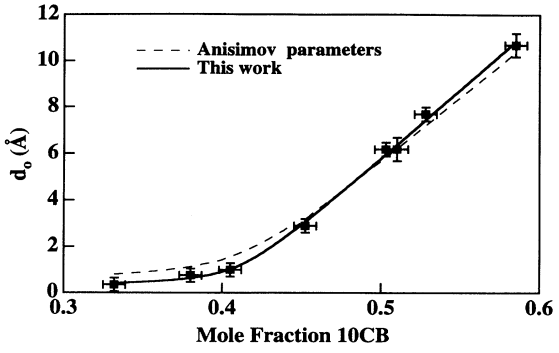


FIG. 10. Capillary-length measurements for mixtures of 8CB and 10CB. The solid curve is a theoretical fit to the measurements based on Eq. (17). The dashed curve uses instead the parameters that Anisimov *et al.* deduced from the latent-heat data collected by Marynissen *et al.* [12]

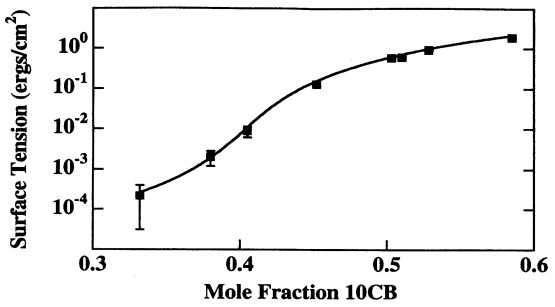


FIG. 11. Surface tension obtained from capillary-length data. The solid line is calculated using the parameters obtained from the fit to the capillary-length measurements using the HLM theory.

TABLE II. Data collected from eight mixtures of 8CB-10CB. The latent heats used to extract $\gamma$ from $d_0$ are calculated using the Anisimov parameters (see Table I).

| Concentration ±0.007 | $d_0$±10% (Å) | $\gamma$ (ergs/cm$^2$) | $L$ (J/cm$^3$) |
|---|---|---|---|
| 0.332 | 0.35 | 2.2e-4 | 0.018 |
| 0.380 | 0.75 | 2.0e-3 | 0.061 |
| 0.405 | 1.0 | 8.8e-3 | 0.13 |
| 0.452 | 2.9 | 0.13 | 0.40 |
| 0.503 | 6.2 | 0.58 | 0.82 |
| 0.510 | 6.2 | 0.60 | 0.88 |
| 0.528 | 7.7 | 0.91 | 1.0 |
| 0.585 | 10.7 | 1.9 | 1.5 |

concentrations of the liquid-crystal mixture in a temperature gradient, an $NA$ interface was pinned to a surface defect on the substrate. The resulting shape of the interface was predicted using the Gibbs-Thomson effect and a fit to this shape gave the capillary-length information. The data, when interpreted using the free energy $F(\psi)$, indicate clearly the presence of a negative cubic term in $\psi$. This term is forbidden by symmetry and analyticity conditions in a single-order-parameter theory, but the HLM calculation, which considers the coupling of two order parameters $\psi$ and $\delta\mathbf{n}$, implies an effective free-energy term of just this form. Our results thus confirm the conclusion of Anisimov, Cladis, and collaborators that the HLM theory is valid near a Landau tricritical point in the $NA$ phase diagram. In addition, we have deduced values for the $NI$ surface tension, which span four orders of magnitude. Our method allows for measurements using very small quantities of material (< 1 mg) and gives results for very small surface tensions ($10^{-4}$ dyn/cm). As yet, neither we nor anyone else has seen any experimental evidence for the tricritical point that Monte Carlo simulations predict for more strongly type-II smectics (i.e., for materials with smaller $T_{NA}/T_{NI}$) or for any deviations that call into question the assumptions of mean-field theory used in writing out both the underlying Landau theory and HLM's modification of it. (Here we refer of course to evidence gathered from measurement of jumps in thermodynamic quantities. Much evidence for scaling behavior beyond mean field has been observed on nominally second-order materials [1].) This points out a need for systematic measurements of even weaker first-order transitions. Our implementation of the "cusp method" was limited by interfacial pinning to the sample's glass plates rather than by the optical resolution of our microscope. It would be interesting to see whether using a different experimental geometry would allow measurements of smaller cusps in smaller temperature gradients, giving access to even smaller capillary lengths.

## ACKNOWLEDGMENTS

This work was partially funded by the National Science and Engineering Research Council (Canada). P. O. and J. B. acknowledge finanical support from NATO. A. M. had financial support from NSERC. J. B. had financial support from the Alfred P. Sloan Foundation. We thank M. Wortis and M. Plischke for helpful conversations and M. Gingras for reading and commenting on the manuscript.

## APPENDIX A: WHY A SCRATCH MAKES A CUSP

Here we consider the effects that a rough substrate will have on a smectic liquid crystal. As discussed above in Sec. III, for small roughnesses, we expect that the smectic layers next to the surface will conform to the substrate profile, at the cost of some elastic distortion energy [1]. For large roughnesses, the smectic will melt to a nematic phase, for which the elastic distortion energy is much smaller (as we shall show below). The tradeoff that we wish to calculate is then between the smectic elastic distortion energy and the extra free energy required to convert the smectic back to a nematic.

We model the rough surface by a sinusoidal profile of wavenumber $m$ and amplitude $u_0$ along the $x$ direction. The $z$ direction is perpendicular to the substrate. The elastic energy of a smectic-$A$ phase is given by

$$F_A = \int \left[ \frac{1}{2} B \left( \frac{\partial u}{\partial z} \right)^2 + \frac{1}{2} K \left( \frac{\partial^2 u}{\partial x^2} \right)^2 \right] dV, \qquad \text{(A1)}$$

where $B$ is the compression modulus of the smectic layers and $K$ is the Frank splay constant, which determines the energy cost of bending layers. Setting $\delta F/\delta u$ to zero, we obtain the Euler equation

$$\frac{\partial^2 u}{\partial z^2} - \lambda^2 \frac{\partial^4 u}{\partial x^4} = 0, \qquad \text{(A2)}$$

where $\lambda \equiv \sqrt{\frac{K}{B}}$ is a length that is roughly the smectic layer spacing ($\approx$ 30 Å). In a semi-infinite geometry, the solution to Eq. (A2) is

$$u = u_0 \cos(mx) e^{-az}, \qquad \text{(A3)}$$

where $a = \lambda m^2$. To estimate the free energy per unit area of a finite-thickness sample, we substitute the elastic distortion for the semi-infinite geometry [Eq. (A3)] into Eq. (A2) and integrate over the finite vertical thickness of

the sample. In our estimate, we choose the sample height $h_c$ to be the decay length of the semi-infinite solution. On the one hand, this allows us to extend the integral to infinity without significant error. On the other hand, it allows us to claim that the elastic distortion energy is more or less uniformly distributed throughout the entire sample. We also need to average over one wavelength of the distortion in the $x$ direction ($2\pi/m$). Putting all of this together, we have

$$F_A \approx \frac{m}{2\pi}\int_0^{2\pi/m} dx \int_0^{\infty} dz \left[\frac{1}{2}Bu_0^2a^2\cos^2 mx\, e^{-2az} + \frac{1}{2}Ku_0^2m^4\cos^2 mx\, e^{-2az}\right] \quad \text{(A4)}$$

$$= \frac{u_0^2m^2}{2\lambda}\sqrt{KB} = \frac{\theta_0^2}{4}\sqrt{KB}, \quad \text{(A5)}$$

where $\theta_0 = u_0 m$ is the maximum angle away from the vertical that a director molecule is forced to adopt at the surface.

One can do a similar calculation for the elastic energy of a nematic liquid crystal anchored to a wavy substrate. In this case, the free energy is (in the one-constant approximation)

$$F_N = \int \frac{1}{2}K\left[\left(\frac{\partial\theta}{\partial x}\right)^2 + \left(\frac{\partial\theta}{\partial z}\right)^2\right] dV, \quad \text{(A6)}$$

where $\theta$ is the local molecular orientation (here confined to the $xz$ plane). The Euler equation is $\nabla^2\theta = 0$, whose solution in a semi-infinite geometry is

$$\theta = \theta_0 \cos mx e^{-mz}. \quad \text{(A7)}$$

Following the smectic calculation, we find

$$F_N = \frac{Km\theta_0^2}{4}. \quad \text{(A8)}$$

Next we note that the free-energy cost of remaining nematic at a temperature $\Delta T$ below the transition temperature is just $\Delta F_{NA} = L_{NA}\left(\frac{\Delta T}{T_{NA}}\right)h_c$. (Again, the estimate is for the latent heat per unit area of a sample of thickness $h_c$.)

To decide whether the sample is nematic or smectic over the scratch at a given temperature, we balance these free energies, leading to

$$L_{NA}\frac{\Delta T}{T_{NA}}h_c + \frac{Km\theta_0^2}{4} = \frac{\theta_0^2}{4}\sqrt{KB}. \quad \text{(A9)}$$

Typical parameter values are $h_c \approx 1.5\times10^{-3}$ cm (above this thickness, we observed variations in the capillary length), $T_{NA} = 317$ °C, $K \approx 10^{-6}$ dyn, $B \approx 10^8$ ergs/cm [1], $\theta_0 \approx 0.3$ rad, and $L \approx 10^6$–$10^7$ ergs/cm$^3$. From AFM profiles of various scratches, we estimate that the roughness wave number $m$ is typically on the order of inverse micrometers ($m \approx 6\times10^4$ cm$^{-1}$). We note that at the relevant wave numbers $m$, we have $\sqrt{KB} \gg Km$ so that the smectic distortion energy dominates over the nematic distortion energy, as claimed above. We thus have

$$\Delta T \approx T_{NA}\left(\frac{\theta_0^2}{4h_cL_{NA}}\right)\sqrt{KB}. \quad \text{(A10)}$$

The transition temperature drop is then about 0.01 °C. In a temperature gradient of about 10 °C/cm, this translates to 10 $\mu$m, which is of the order of the depth of the cusps seen in this experiment.

For the nematic-isotropic ($NI$) interface, we have $L_{NI}\left(\frac{\Delta T}{T_{NI}}\right)h_c = \frac{Km\theta_0^2}{4}$, or

$$\Delta T = T_{NI}\left(\frac{\theta_0^2}{4h_cL_{NI}}\right)Km\,. \quad \text{(A11)}$$

Using the $NI$ latent heat of $3\times10^7$ ergs/cm$^2$, we find $\Delta T \approx 10^{-5}$ °C, or a scale of about 0.01 $\mu$m. Since $h \gg 0.01$ $\mu$m, we see no cusp where the scratch crosses the $NI$ interface. Again, the essential point is the relative fragility of the smectic layers to disruption by surface roughness.

## APPENDIX B: THICKNESS DEPENDENCE OF THE CAPILLARY LENGTH

As mentioned at the end of Sec. V, one might worry whether the thickness of the sample $h$ affects the values of $d_0$ deduced from the cusp image. Indeed, we observed that upon increasing $h$ from 12.5 $\mu$m to up to 50 $\mu$m, the apparent capillary length would vary by a factor of 5. For the 50-$\mu$m samples, the model gave a particularly poor fit to the interface. Because the scratch was on

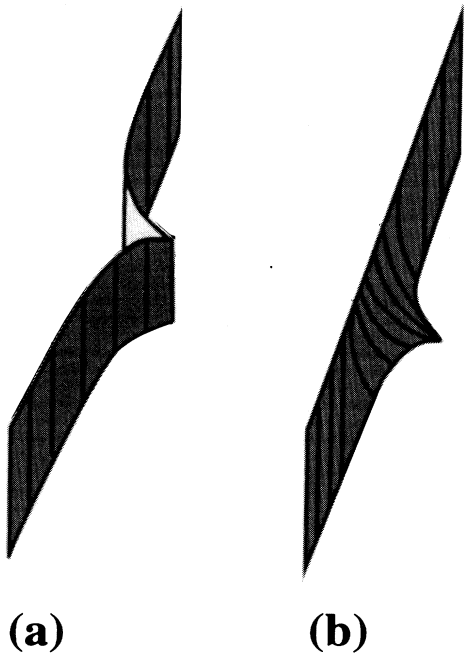


FIG. 12. (a) For thin samples, the effect of a scratch on one glass plate extends throughout the sample thickness. (b) For thick samples ($h > 15$ $\mu$m), the scratch pins only the bottom of the interface, leading to the vertical profile sketched here.

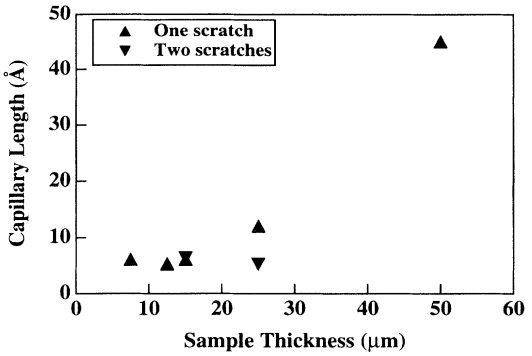


FIG. 13. Effects of thickness on capillary length in samples where the interface is pinned to one surface of the cell and where the interface is pinned to both surfaces. $X = 0.51$.

only one of the glass plates, the interface was pinned on only one side of the sample. In the extreme case, this would mean that the shape of the interface was a straight line on the top plate and a cusp shape on the bottom plate, with the meniscus interpolating between these extremes in between. This implies a curvature in the vertical direction. (See Fig. 12.) Since the calculation of the cusp shape assumes a constant vertical-curvature profile, the derived functional form of the cusp would not be valid here.

Although thick samples gave varied values for $d_0$, one can hope that for thin enough samples, the values deduced for $d_0$ would become independent of sample thickness. We now show experimentally that this is indeed the case. Two different methods were used to establish this. First, the nominal thickness was varied from 7.5 $\mu$m to 50 $\mu$m to see whether there was a range of thickness in which the capillary length was not affected. Second, both plates of the sample were scratched and the scratches aligned under a microscope to within a couple of microns. The interface was then pinned to the top and bottom surfaces, minimizing curvature variation in the vertical direction.

For samples with only one scratch, the capillary length was more or less constant for thicknesses in the range 7.5 $\mu$m $< h <$ 15 $\mu$m. It was larger for 25 $\mu$m and thicker samples. (See Fig. 13.) For fits to interfaces in the 50-$\mu$m samples, the point of contact between the interface and the scratch implied by the fit was far from the contact point determined by eye. In other cases, the two coincided.

Samples with two scratches were made for $h = 15$ $\mu$m and 25 $\mu$m. The values of $d_0$ deduced for these samples agreed with those found using single-scratch samples with $h \leq 12.5$ $\mu$m. (See Fig. 13.) This confirmed that using thick samples with only one scratch did affect the capillary-length measurements, but keeping $h < 15$ $\mu$m avoided the problem.

## APPENDIX C: EFFECTS DUE TO MIXTURES AND IMPURITIES

The discussion in the body of the paper assumed implicitly that the material being studied was pure. Obviously, since we used a mixture of two different liquid crystals, this is not true. Slightly less obviously, these materials will themselves have small amounts of impurities. The presence of several components raises a number of questions about our analysis. We shall argue below that all of these concerns turn out to be unimportant for us and that we are justified in treating the experimental data as if it pertained to a pure material. We justify this conclusion by considering the following questions.

(1) What are the actual levels of impurities and what are their effects on the equilibrium phase diagram (Fig. 1)?

(2) Does the shape of the cusp change?

(3) Is the form of the free energy changed by the impurities?

(1) Our mixtures of 8CB and 10CB used materials supplied by BDH, Ltd. The manufacturer claims that the primary impurity in the material as supplied is water, whose saturation concentration at room temperature is about 0.15 mol%. We assessed the purity of our materials directly by measuring the nematic-isotropic melting range of the base components 8CB and 10CB. (See Fig. 14.) For 8CB, we found a melting range of not more than 0.2 °C, which could be reduced to about 0.06 °C by heating and pumping on the liquid in a vacuum dessicator. The logical assumption is that the difference in melting ranges occurs as volatile impurities (particularly water) are pumped off, while the portion that could not be pumped off corresponds to nonvolatile impurities. Using the van t'Hoff law for ideal solutions, one has that the amount of impurities is approximately $[X_{imp} = \Delta T_{NI}/(dT_{NI}/dX_{imp})][k/(1-k)]$, where $\Delta T_{NI}$ is the $NI$ coexistence range and $dT_{NI}/dX_{imp}$ is the $NI$ liquidus slope for the impurity. Using $\Delta T_{NI} = 0.2$ °C, $k \approx 0.8$, and $dT_{NI}/dX_{imp} \approx -1$ °C/mol % [37], we estimate $X_{imp} \approx 0.8$ mol %. Because the value of $\Delta T_{NI}$ varies only slightly with the mixture concentration $X_{10CB}$, we conclude that it reflects the segregation of impurities rather than that of the liquid-crystal molecules themselves. In particular, we conclude that any compositional effects are dominated by the impurities (water, etc.) rather than by demixing of the 8CB and 10CB.

We also measured the $NA$ coexistence range $\Delta T_{NA}$ (cf. Fig. 14) and found that it varied between 0.03 and

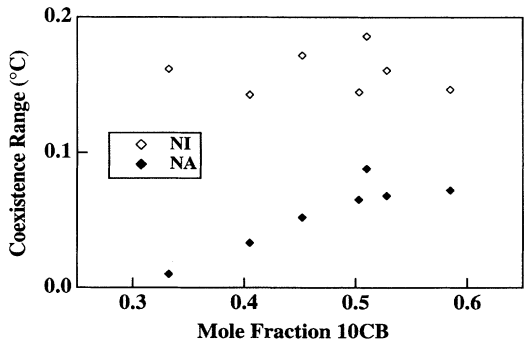


FIG. 14. Measured coexistence ranges for the $NA$ and $NI$ transitions. Compare [27] for a discussion of the measurement technique.

0.08 °C, depending on the mixture concentration. From the phase diagram (Fig. 1), we estimate the local slope of the liquidus line to be $dT_{NA}/dX_{10CB} \approx 0.2$ °C/mol %. In contrast to the $NI$ case, $\Delta T_{NA}$ does depend on the mixture concentration. This is to be expected near a critical point, since the free-energy difference of an impurity molecule in one or the other phase goes to zero. If we assume that $\Delta T_{NA}$ arises entirely because of the impurities, then we can deduce an $NA$ impurity partition

$$k_{imp} \equiv \frac{X_A}{X_N} = 1 + \frac{X_A - X_N}{X_N} \approx 1 + \frac{\Delta T_{NA}}{100 \frac{dT_{NA}}{dX_{10CB}} X_N} \approx 1.002. \quad \text{(C1)}$$

(The factor of 100 converts the liquidus slope from mol % to mol fraction.) The jump in impurity concentration across the interface is thus very small.

(2) Having estimated the magnitude of the composition jumps and of the overall impurity concentrations, we now ask whether these can affect the shape of the cusp. If a steady state is maintained, the answer would be no. Jumps in impurity and 10CB concentration across the interface do lead to a shift in the melting temperature, as discussed in point (1) above. As long as this shift is uniform, the only effect will be a uniform displacement of the interface. However, if there is a gradient of concentration along the $NA$ interface, the cusp shape will change. Melo considered one cause of a concentration gradient, that due to motion of the interface (caused by fluctuations in the temperature regulation), and found that the shape was changed significantly only when the thermal length $\Delta T_{NA}/G$ is much less than the diffusion length characterizing the concentration gradient ($D/v$, where $D$ is the diffusion coefficient and $v$ is the typical interface velocity) [38]. We can estimate this front velocity to be $v \approx (dT_{reg}/dt)/G$, where $dT_{reg}/dt$ is the rate of change of temperature in the vicinity of the $NA$ front due to temperature-regulation fluctuations. We conclude that the cusp shape will be largely unchanged then as long as

$$G \gg \left[ \frac{\Delta T_{NA} \frac{dT_{reg}}{dt}}{D} \right]^{1/2}. \quad \text{(C2)}$$

Using $\Delta T_{NA} = 0.08$ °C, $D = 10^{-6}$ cm$^2$/s, and noting that the temperature fluctuates 7 mK over 2 h, we find that our temperature gradient $G$ should be greater than about 0.3 °C/cm, which is about ten times smaller than our smallest gradients. Note that the presence of $dT_{reg}/dt$ in Eq. (C2) suggests that it is important to minimize not just the temperature fluctuations, but also their rate. For this reason, we chose to control the temperature of both blocks by water baths, which have long time constants.

(3) The last question is how the impurities change the form of the free energy used to calculate the capillary length. Anisimov [39] considered this question and concluded that impurities act as a scalar field in much the same manner as the nematic order parameter considered in Sec. II. Using a mixture and having impurities is thus expected to change the $A$ and $C$ coefficients in Eq. (4), but not to alter its form. Thus we conclude that we are justified in treating our mixture, with its small amount of impurities, as a single-component system.


[1] P. de Gennes and J. Prost, *The Physics of Liquid Crystals, International Series Of Monographs on Physics*, 2nd ed. (Clarendon, Oxford, 1993).
[2] M. A. Anisimov, Mol. Cryst. Liq. Cryst. A **162**, 1 (1988).
[3] W. G. Bouwman and W. H. de Jeu, in *Modern Topics in Liquid Crystals,* edited by A. Buka (World Scientific, Singapore, 1993), p. 161.
[4] C. Garland and G. Nounesis, Phys. Rev. E **49**, 2964 (1994).
[5] K. K. Kobayashi, Phys. Lett. **31A**, 125 (1970).
[6] P. de Gennes, Solid State Commun. **10**, 753 (1972).
[7] W. L. McMillan, Phys. Rev. A **4**, 1238 (1971).
[8] B. I. Halperin, T. C. Lubensky, and S. K. Ma, Phys. Rev. Lett. **32**, 292 (1974); B. I. Halperin and T. C. Lubensky, Solid State Commun. **14**, 997 (1974).
[9] C. Dasgupta and B. I. Halperin, Phys. Rev. Lett. **47**, 1556 (1981).
[10] C. Dasgupta, Phys. Rev. Lett. **55**, 1771 (1985).
[11] J. Bartholomew, Phys. Rev. B **28**, 5378 (1983).
[12] H. Marynissen, J. Thoen, and W. V. Dael, Mol. Cryst. Liq. Cryst. **124**, 195 (1985).
[13] M. Anisimov *et al.*, Mol. Cryst. Liq. Cryst. B **150**, 399 (1987).
[14] M. A. Anisimov *et al.*, Pis'ma Zh. Eksp. Teor. Fiz. **45**, 336 (1987) [JETP Lett. **45**, 425 (1987)].
[15] D. Brisbin, R. DeHoff, T. Lockhart, and D.L. Johnson, Phys. Rev. Lett. **43**, 1171 (1979).
[16] M. Huster, K. Stine, and C. Garland, Phys. Rev. A **36**, 2364 (1987).
[17] P. Cladis *et al.*, Phys. Rev. Lett. **62**, 1764 (1989).
[18] M. Anisimov *et al.*, Phys. Rev. A **41**, 6749 (1990).
[19] R. Schaefer, M. Glicksman, and J. Ayers, Philos. Mag. **35**, 725 (1977).
[20] P. Oswald, J. Phys. (Paris) **49**, 1083 (1988).
[21] P. G. de Gennes, Mol. Cryst. Liq. Cryst. **21**, 49 (1973).
[22] P. G. de Gennes, Solid State Commun. **10**, 753 (1972).
[23] G. Barbero and G. Durand, J. Phys. II **1**, 651 (1991).
[24] B. Caroli, C. Caroli, and B. Roulet, in *Solids Far From Equilibrium*, edited by C. Godrèche (Cambridge University Press, Cambridge, 1992), Chap. 2, pp. 184–186 and 285–286.
[25] P. Nozières, in *Solids Far From Equilibrium*, edited by C. Godrèche (Cambridge University Press, Cambridge, 1992), Chap. 1, pp. 6–7.
[26] W. Press, S. Teukolsky, W. Vetterling, and B. Flannery, *Numerical Recipes in* FORTRAN. *The Art of Scientific*

*Computing*, 2nd ed. (Cambridge University Press, Cambridge, 1992), pp. 355–360.
[27] N. Tamblyn, M.Sc. thesis, Simon Fraser University, 1994.
[28] Neslab Model RTE-110d refrigerated water-bath circulator. Neslab Instruments, Inc., Newington, NH 03801.
[29] Olympus IMT-2 inverted microscope. Olympus Corp., Lake Success, NY 11042-1179.
[30] Pulnix TM-7CN CCD camera. Pulnix Corp., Sunnyvale, CA 94086.
[31] PixelGrabber and PixelPipeline acquisition boards. Perceptics Corp., Knoxville, TN 37933.
[32] NIH Image is a public-domain image processing program.
[33] Berger Lahr VRDM 564 stepping motor with microstepping control. Berger Lahr Motion Technology, Inc., Plymouth, MI 48170.
[34] Model MHR 500 LVDT with ATA-101 analog transducer amplifier. Schaevitz Engineering, Pennsauken, NJ 08110.
[35] W. Press, S. Teukolsky, W. Vetterling, and B. Flannery, *Numerical Recipes in* FORTRAN. *The Art of Scientific Computing* (Ref. [26]), pp. 678–683.
[36] A. Dougherty and J. Gollub, Phys. Rev. A **38**, 3043 (1988).
[37] J. Bechhoefer, A. J. Simon, A. Libchaber, and P. Oswald, Phys. Rev. A **40**, 2042 (1989).
[38] F. Melo, Ph.D. thesis, Université Claude-Bernard (Lyon I), 1991, pp. 40–41.
[39] M. A. Anisimov, JETP Lett. **37**, 11 (1983).

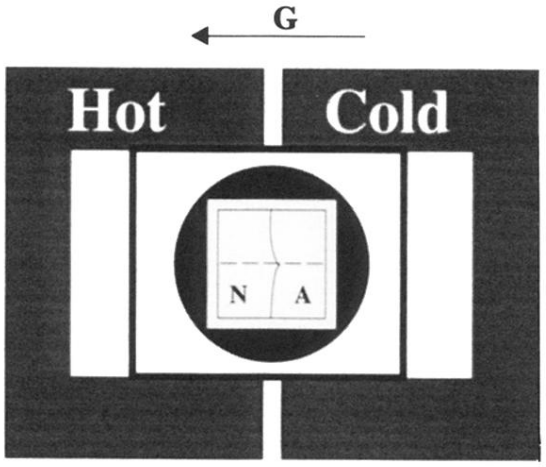


FIG. 4. Schematic top view of the temperature-gradient stage. The sample is surrounded by a disk, so that it may be rotated to align the scratch with the temperature gradient.

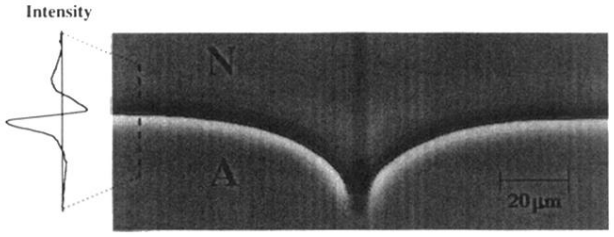


FIG. 5. Measured interface coordinates superimposed on photograph of cusp. $X = 0.585$, $h = 12.5$ $\mu$m, phase-contrast microscopy. The vertical graph shows the light-intensity profile perpendicular to the interface.

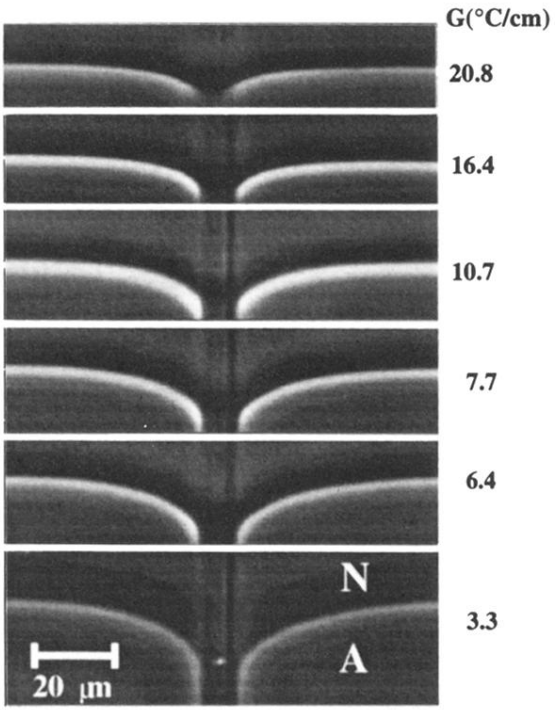


FIG. 6. Cusps in different temperature gradients. $X = 0.503$, $h = 12.5$ $\mu$m, phase-contrast microscopy.